

# Analytical model for ArF photoresist shrinkage under scanning electron microscopy inspection

Guy Ayal and David Andelman<sup>a)</sup>

Raymond and Beverly Sackler School of Physics and Astronomy, Tel Aviv University, Ramat Aviv, Tel Aviv 69978, Israel

Yachin Cohen

Wolfson Department of Chemical Engineering, Technion-Israel Institute of Technology, Technion City, Haifa 32000, Israel

(Received 4 September 2008; accepted 8 June 2009; published 28 July 2009)

Linewidth slimming is a phenomenon occurring specifically in photolithography of 193 nm wavelength (ArF) radiation. Photoresists for this wavelength appear to lose volume when exposed to electron-beam radiation, as when scanned in scanning electron microscopy for critical dimension (linewidth) measurement. This work is an attempt to understand this “shrinkage” from a polymer physics point of view. More specifically, the authors try to check the applicability of free volume theory in polymer systems by calculating some relevant physical properties, assuming that the exposure to e-beam creates an external hardened shell for the material bulk, and continued exposure will deliver heat into the polymer enclosed in a confined space. The authors’ main conclusion is that the free volume loss (annealing) shows qualitative resemblance to experiment, but this effect exclusively is *not* a sufficient quantitative explanation for the observed shrinkage. A possible explanation for this discrepancy is that their model is limited due to unknown material parameters, or that the annealing is coupled with other effects such as “wringing” solvent out. © 2009 American Vacuum Society. [DOI: 10.1116/1.3167364]

## I. INTRODUCTION

Linewidth slimming (LWS) has been considered a major problem in IC manufacturing since the introduction of 193 nm radiation photolithography, around 1999. As IC devices and chips grew smaller, the 193 nm lithography became the backbone of the industry, and LWS was declared as one of seven main hindrances for further scaling down.<sup>1,2</sup>

LWS is defined as the shrinking effect of patterned photoresist during scanning electron microscopy (SEM) measurement.<sup>3</sup> Varying according to resist chemistry platform and SEM conditions, the effective linewidth reduction can reach, in extreme cases, up to 20% of original *critical dimension* (CD) (resist linewidth). This means loss of up to 40% of the original material volume because the actual reduction is two dimensional: in the CD direction ( $x$ -axis) and in its height ( $z$ -axis), but not in the longitudinal extended direction ( $y$ -axis) as the line length is much longer than the scale of SEM-affected area.<sup>4</sup>

Most of the studies on “linewidth slimming” were done using CD-SEM tools, generating one-dimensional data only. Therefore, in the term LWS, as described above, only the width of the patterned line is referred to. However, some cross-sectional SEM images and atomic force microscopy (AFM) scans showed this effect to be two dimensional in nature.<sup>5</sup> The extent of shrinkage along the  $z$ -axis (height) was shown in a few occasions to be about the same as along the  $x$ -axis (width), but these were only specific examples, with no quantitative rigorous comparison reported.

As mentioned above, LWS for different photoresists varies according to the materials used as compound resins. Methacrylate resists, which are the most common materials mostly because of their price, exhibit faster shrinkage than other materials such as cycloolefin-maleic anhydride (COMA).

Kudo *et al.*<sup>6</sup> measured the LWS effect and fitted it to a sum of three exponential decays, suggesting that three different processes take place on three very different time scales: (i) a very fast (half-life time of 2–8 s) process affecting only the very outer rim of the material; (ii) A slower process (half-life time of 30–40 s) affecting the shrinkage of the main bulk of the material; (iii) a very slow (half-life time larger than 10<sup>4</sup> s) process characterizing the decay of the entire material,

$$W = a_1 \exp\left(-\frac{\ln 2}{\tau_1} t\right) + a_2 \exp\left(-\frac{\ln 2}{\tau_2} t\right) + a_3 \exp\left(-\frac{\ln 2}{\tau_3} t\right), \quad (1)$$

where  $W$  depicts the ratio between remaining CDs and original CDs, while  $a_1, a_2, a_3$  and  $\tau_1, \tau_2, \tau_3$  are the relative amplitudes of the three processes and their half-life times, respectively, and depending on resist chemistry.

Additional conditioning of the resist, by baking it for longer times than are conventionally done in the lithographic process, can decrease the effect of the two fast-decay processes,<sup>7</sup> while leaving a wider line for the final decay. For example, overall shrinkage after 10 min of exposure to SEM can be reduced by 25%. Kudo *et al.*<sup>6</sup> also found that the use

<sup>a)</sup>Electronic mail: andelman@post.tau.ac.il

of a more volatile solvent in resist preparation can reduce the size skimming of the second stage by about 50%. This is assumed to be due to less (or no) solvent remaining in the material when it reaches the SEM so no solvent evaporation takes place.

When examining the shrinkage of the main bulk of the material (the second stage described above), it is seen that this stage is responsible for up to 14% of the width loss. Assuming that loss of height is about the same as loss of width that would make up to 30% volume loss for infinitely long stripes.

Previous attempts to explain this phenomenon mainly focused on solvent evaporation.<sup>4,6</sup> Clearly, some of the shrinkage is caused directly by solvent evaporation because changing to a more volatile solvent causes the resist to shrink less, and so does baking the material. However, even taking the reductions by solvent replacement and baking to be additive (an assumption that cannot be fully justified) still leaves a loss of about 10% in volume (or 6% width) left as main bulk shrinkage, with a half-life time of 30–40 s.

In this article, we try to apply the fundamental physics of pressure-volume-temperature (P-V-T) relations in polymers, and explore a previous suggestion of polymer annealing<sup>1,7</sup> (loss of free volume) as a possible mechanism responsible to linewidth shrinkage. More specifically, we study in detail how much free volume loss is possible in methacrylate-based photoresist exposed to SEM radiation. The thermodynamical parameters of polymethyl methacrylate (PMMA) are used in the present work due to their availability in accurate measurements, even though this specific methacrylate is not the one usually used for optical lithography, but rather for e-beam and ion-beam lithographies.<sup>8</sup> It is reasonable to assume that the differences between PMMA and the other, more commonly used, methacrylates have little or no qualitative importance. The study presented here gives an estimate for the upper bound of the amount of volume lost via annealing, and elucidates whether or not annealing is a suitable explanation for this phenomenon. In Sec. II, the theoretical model is described, first through a short review of the theoretical background and description of the model setup, followed by an elaboration of our analytical solution. In Sec. III, we describe in detail the numerical and experimental results, followed by a comparison between the two. Conclusions are presented in Sec. IV, in which we also suggest possibilities for future studies.

## II. MODEL

### A. Free volume theory

Studies of mechanical properties of polymers in their glassy state have grown considerably over the past decades. As the use of solid plastic materials in industry and households expanded, so did the need to understand the constitutive properties of amorphous glassy polymers, and especially their special mechanical behavior. Since some level of flow exists even in the solid state of amorphous polymers, many studies have concentrated on rheological properties of polymer glasses in different conditions.<sup>9,10</sup>

Various studies<sup>11–13</sup> made it clear that the mechanical properties of glassy polymers strongly depend on sample thermal history and past conditions, besides their current thermodynamical ones. One of the relevant observations is that a polymer glass, annealed for long times at a temperature *below* the glass transition temperature, slowly changes its mechanical characteristics, such as density and Young modulus.<sup>9</sup> Although such behavior has been well known in metals, the extent is far larger in glassy polymers, where the material actually loses measurable amounts of volume via compaction.<sup>14,15</sup> It has also been seen that there is a correlation between changes in specific volume and changes in dielectric and mechanical properties.<sup>13</sup>

The main theory explaining this intriguing behavior is the *free volume theory*. This theory, developed initially for all glassy materials,<sup>16,17</sup> was further applied to glassy polymers.<sup>18</sup> It stipulates that the glassy material includes considerable free volume in the form of *vacancies* between the amorphously distributed molecules. In polymers the effect is significantly stronger because much more free volume is trapped between polymer chains due to the limitations on their movement during solidification.

Free volume in polymers was originally introduced to theoretical studies of polymer melts, as an explanation of viscosity variation at various temperatures above the glass transition.<sup>14</sup> Later, it was found that free volume is a key parameter to understand also the solid glass phase. It has been shown, both theoretically and experimentally,<sup>18</sup> that upon cooling a polymer below its glass transition  $T_g$ , the volume contraction is consistent with thermodynamics only if one considers “excess” volume. Collaborating evidence was presented when specific volume  $V_s$  measurements yielded significantly higher values than theoretical equilibrium values. The main conclusion drawn was that this “solid” glass state of polymeric material below the glass transition is actually metastable and includes a lot of “frozen-in” free volume.

Experimental evidence for this conclusion can be seen in Fig. 1. The solid line represents the experimental results of specific volume  $V_s$  in PMMA after the material settled into what is seemed as an attainable equilibrium. Results below  $T_g \approx 360$  K were measured after a prolonged (over 3 h) annealing at each temperature, in order to approach as much as possible equilibrium conditions. The dashed line in the figure represents the thermodynamic equilibrium values of the occupied volume. A clear discrepancy (relative difference of 2%) between the theoretical equilibrium values and the experimental ones can be seen in Fig. 1. It is quite clear from these results that the actual free volume as obtained in the cooling experiments is a considerable fraction (between 1.5% in this case and up to 3%–5% in others) of the overall volume.

The existence of “residual” free volume in polymer glass is explained<sup>9</sup> by considering that random thermal vibrations in the solid are unlikely to destroy the network disorder as embodied by the vacancy distribution. As the material passes through the glass transition, the reduced mobility level does

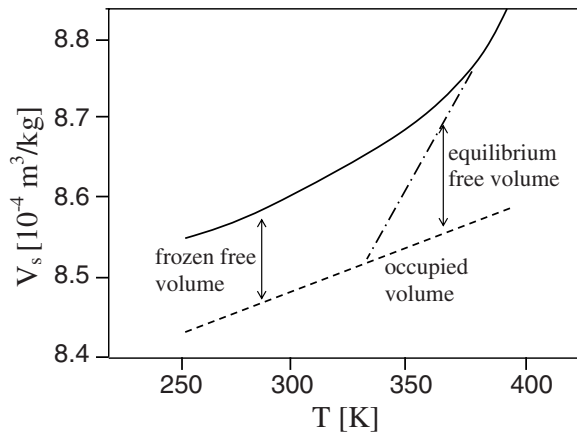


FIG. 1. (Color online) Experimental data for occupied and actual specific volume ( $V_s$ ) in PMMA. The dashed line denotes the occupied volume, the dotted-dashed line is the equilibrium free volume, derived from the material viscosity and the full line is the experimental results (adapted from Ref. 18).

not allow for molecules to find vacancies and fill them. The result is that free volume almost ceases to change during glass transition and is frozen in.<sup>13</sup>

Residual free volume is strongly correlated<sup>11,13,19,20</sup> with changes in the glass transition temperature and other mechanical properties of polymers such as the increase in density and bulk modulus when decreasing the cooling rate of the liquid into the glassy state. Inspection of experimentally measured  $P$ - $V$ - $T$  diagrams of polymeric materials would reveal strong dependence of  $V$ - $T$  curves on the isobaric pressure.<sup>21-24</sup> Moreover, in amorphous polymers, the isobars continue into the glassy solid region without any extreme changes.

In Fig. 2 experimental results for PMMA, obtained by Schmidt and Maurer<sup>22</sup> are presented. Between lines A and B in this figure, a glass is formed from the melt. This glass does not possess the same thermodynamic history as the material

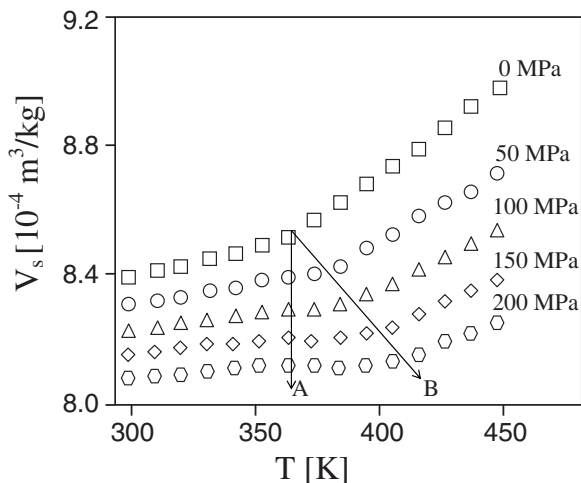


FIG. 2. Experimental diagram (isobars) for PMMA cooled from the liquid state (melt). Five different isobars with pressures 0, 50, 100, 150, and 200 MPa, respectively, are indicated by different symbols (reproduced from Ref. 22).

originally loaded, and it shows different behaviors for any small condition change that can be drawn in this “wedge.”

One very important conclusion from these studies is that pressure history of glassy polymer has a strong effect on its current engineering properties. In particular, pressure applied on the material in the liquid phase will have a large effect on the polymer even after solidification and/or after the pressure is lowered.

Moreover, the dependence of specific volume  $V_s$  on pressure during solidification can be measured. For commercially used PMMA the fitted dependence was derived (for  $T = 296$  K) in Ref. 22,

$$V_s \approx V_{s0} \exp[-P/P_0], \quad (2)$$

with

$$V_{s0} = 8.4 \times 10^{-4} \text{ m}^3/\text{kg},$$

$$P_0 = 5000 \text{ MPa},$$

where  $V_s$  is the measured specific volume,  $P$  is the pressure of the isobar along which the melt is being cooled,  $V_{s0}$  is specific volume at atmospheric pressure and room temperature, and  $P_0$  is the pressure fit parameter.

The explanation for the history dependence of the pressure is the same as for the thermal history. Namely, the conditions of the melt state define the amount of free volume that is frozen into the material. Once the glass transition has taken place, the polymer deviates from its thermodynamic equilibrium and settles into a metastable state that cannot further adjust according to the present system conditions.

## B. Model setup of linewidth slimming

Different thermodynamic models for glassy polymers have been proposed over the years. The most explicit way to explain polymer behavior would be to create a full molecular dynamic simulation.<sup>25,26</sup> In those models the main expected results are the spatial location of every monomer along the chain, in order to check reactions to various manipulations.

More coarse grained models, such as the one developed here, are based on a thermodynamic approach, where all calculations are done on a macroscopic level, and the polymeric structure is taken into account only through its thermodynamic and mechanical parameters. From these calculations, it is possible to simulate even nonlinear properties of polymers, such as their viscoelasticity.<sup>27,28</sup>

The physical system that our model addresses is described schematically in Fig. 5. Practically all controlled experiments in LWS were done on photoresist lines extending across a silicon substrate, reducing the setup to a two-dimensional one (the third dimension, as mentioned above, is in practice of infinite extent). For this work, we further reduced the problem to a one-dimensional one with variations only along the height ( $z$ -axis). This further simplification may bear some artifacts on the results, as we take only the directionality of the e-beam into account, and not that of the photoresist line. In previous publication<sup>29</sup> resist shrinkage was reported to occur when exposing resist blankets (thin uniform layers,

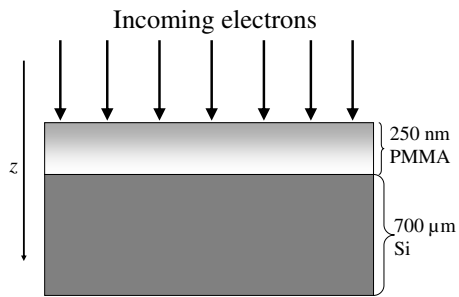


FIG. 3. Schematic setup of electron bombardment of the specimen during SEM observation. The scales of the PMMA layer and the silicon substrate are very different.

with no pattern), but this was only observed qualitatively, and at present no quantitative experimental data is available for comparison. Changes in electron incidence on top on walls of two-dimensional structures is assumed to be small, in accordance with data from CD-SEM tool manufacturers,<sup>30</sup> who base the metrology definitions and edge locations on all surfaces receiving similar charging, and install the hardware accordingly.

Consider a layer of 250 nm thick PMMA used as a photoresist for etchable layers in photolithography (e.g., epitaxial silicon for transistor active area). As mentioned above, PMMA is mainly used for e-beam lithography, but is typical for other acrylic materials. We use it here because of the availability of accurate thermodynamical parameters, while assuming that the differences between PMMA and the methacrylates generally used as photoresists [such as 2-methyl-2-adamantanol methacrylate (MAdMA)] will not have a major effect on our conclusions. We will elaborate on this point in Sec. II C

The PMMA layer is placed upon a silicon wafer made of 700  $\mu\text{m}$  thick layer of single-crystal silicon. The entire specimen is now bombarded by electrons from a SEM source, as sketched in Fig. 3, with a flux of 6.7  $\text{pA}/\text{nm}^2$ , at an acceleration voltage of 600 V mimicking normal conditions for standard industry CD-SEMs, such as Hitachi s-9260, AMAT Verity or KLA eCD1-93E.<sup>31</sup>

As the incident electrons are scattered by the atoms of the polymeric layer, most of their kinetic energy is transformed into heat. Very little energy is lost due to emission of secondary electrons because these electrons leave the substrate with an average energy that is about two orders of magnitude less than their incident energy.<sup>32</sup> Furthermore, we also assume that the effective charging of the PMMA layer is negligible, as the number of secondary electrons is approximately equal to that of the incoming electrons, and also because charging of the specimen is often a controlled parameter in CD-SEM measurements.<sup>33</sup> Therefore, the energy deposition distribution as function of penetration depth  $Q(z)$  used for heat transfer equations coincides with a measurable parameter: the charge penetration distribution of incident electrons  $E_D(z)$  which is described in Fig. 4.

As electrons impact the polymer material, they initiate a simultaneous process of both cleavage and cross-linking of

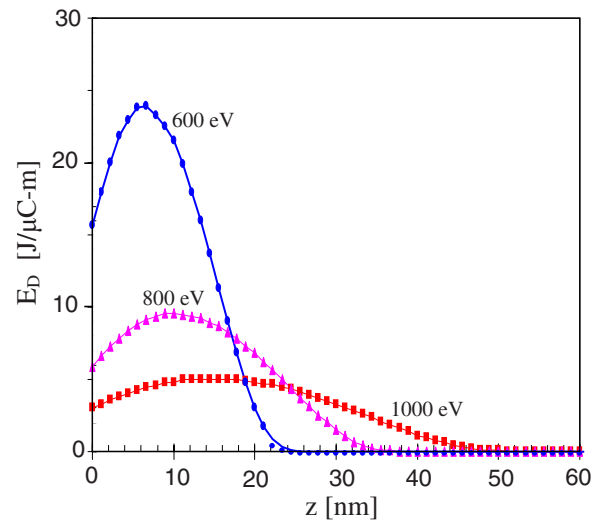


FIG. 4. (Color online) Penetration of electrons to PMMA. Deposited energy of penetrating electrons on a PMMA photoresist specimen as function of the penetration depth. Three levels of acceleration energies are indicated on the figure (reproduced from Ref. 1).

the chains. The layer of material directly exposed to the incoming electrons hardens, creating a tough outer shell on top of the polymer bulk (Fig. 5), leading to heating of the inner polymer core in a confined space.<sup>6</sup> Some evidence for this process was recently given<sup>34</sup> and manifests that chemical changes in the outer polymer layer play a role in LWS. However, this evidence still awaits further verification and detailing. Another model assumption is that the cross-linking enhances the polymer hardness and toughness. Therefore, we expect cross-linked polymer to be resistant to stress, and not to extend when tension is applied. This is in agreement with several studies about mechanical properties of cross-linked polymers.<sup>35</sup>

Yet another assumption is that the cross-linking level at any depth beneath the surface depends on the number of electrons reaching it. This is a rather reasonable outcome, implying that the cross-linked layer is not really a separate layer, but it is rather connected to the polymeric core via a gradual interface. If the inner core loses volume, the outer layer will shrink along with it.

Since the material expands upon heating inside a space confined by the outer shell (as described above), pressure is

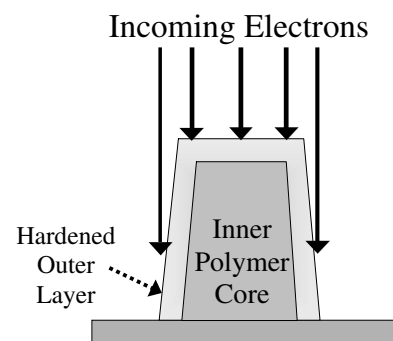


FIG. 5. Schematic illustration of the creation of a hardened outer layer.

bound to rise dramatically. Thermal expansion and isothermal compression are highly affected by specific attributes and exact composition of the sample being measured. In order to have material parameters that are as close as possible to our conditions, we assorted to using data from molecular dynamic simulations rather than experiment. Once the pressure elevation profile is known, we can calculate the specific volume loss (and from there, linewidth slimming) using the experimental results described above.

### C. The model and its solutions

The heat diffusion model is solved numerically. This is done without taking into account any first-order phase transition or chemical reaction because no fundamental changes in the materials involved have ever been observed since the discovery of LWS. Therefore, we fit the energy deposition distribution  $Q(z)$  of the incident electrons with a Gaussian function,

$$Q(z) = \frac{Q_0}{\sqrt{2\pi}} \exp\left[-\frac{(z-z_0)^2}{2\sigma^2}\right], \quad (3)$$

where  $z$  is the penetration depth,  $z_0$  is the depth of average deposition, and  $\sigma$  is the depth dispersion. Both parameters are taken from experimental data<sup>31</sup> to be  $z_0=8$  nm and  $\sigma=0.3$  nm.  $Q_0$  is the overall energy flux, which is defined by  $Q_0=I\phi/A$ . The current  $I$ , landing voltage  $\phi$ , and probing area  $A$  vary according to specific SEM tool specs, and are taken to have the same values used in most LWS experiments:  $I=6$  pA,  $\phi=600$  V, and  $A=0.78$  nm<sup>2</sup>. The latter is the probe area of a circular beam with 1 nm diameter.

The heat that is generated by the incoming electrons then diffuses into the bulk of the material. The inhomogeneous heat diffusion equation<sup>36</sup> depends on energy source term  $Q(z)$  and is written as

$$\frac{\partial^2 T}{\partial z^2} - \frac{1}{\alpha} \frac{\partial T}{\partial t} = -\frac{1}{\kappa} Q(t, z), \quad (4)$$

where  $T$  is the temperature,  $\alpha$  is the thermal diffusivity, and  $\kappa$  is the thermal conductivity. The parameters  $\alpha$  and  $\kappa$  have different values in the polymer layer and silicon substrate. For silicon their values are available in engineering databases,<sup>37</sup>

$$\begin{aligned} \alpha_{\text{Si}} &= 2.6 \times 10^{-6} \text{ K}^{-1}, \\ \kappa_{\text{Si}} &= 1.48 \times 10^{-7} \text{ W nm}^{-1} \text{ K}^{-1}. \end{aligned} \quad (5)$$

PMMA is a widely used material in various engineering applications and its thermal properties are widely known from various studies and engineering databases.<sup>37,38</sup> However, in most such databases the  $\alpha$  and  $\kappa$  coefficients for PMMA are given within a wide range because their specific value depends on the PMMA sample preparation and its thermal and mechanical history. In this work, we used the midrange values for the calculations, and the two extremes for sensitivity checks,

$$\alpha_{\text{PMMA}} = 7 \times 10^{-5} \pm 2 \times 10^{-5} \text{ K}^{-1},$$

$$\kappa_{\text{PMMA}} = 2.09 \times 10^{-10} \pm 0.42 \times 10^{-10} \text{ W nm}^{-1} \text{ K}^{-1}. \quad (6)$$

With  $Q(z)$  of Eq. (3) and the numerical values as given in Eq. (5) and (6), the parabolic partial differential equation [Eq. (4)] can be solved numerically employing a finite difference approximation known as the *implicit method*.<sup>39</sup> The solution is a matrix  $T(z, t)$  of discrete temperature values across the material and through time. We then calculate the pressure profile  $P(z, t)$  and the volume loss for the polymeric layer alone, as the silicon substrate takes no active role in this part.

Recalling the definition of the thermal expansion:  $\alpha_p \equiv (1/V)(\partial V/\partial T)_p$  and bulk compliance:  $\kappa_T \equiv -(1/V) \times (\partial V/\partial P)_T$ , the pressure is calculated using one of the Maxwell identities,<sup>36</sup>

$$\left(\frac{\partial P}{\partial T}\right)_{V,N} = \frac{\alpha_p(T)}{\kappa_T(T)}. \quad (7)$$

In order to integrate the pressure from Eq. (7), we must take into account the temperature dependence of  $\alpha_p$  and  $\kappa_T$ . These coefficients for PMMA at room temperature are given in many engineering databases,<sup>37,38</sup> but their dependence on temperature is usually not given. Therefore, we make use of the results obtained from of explicit molecular dynamics simulation conducted especially for this goal,<sup>40</sup>

$$\begin{aligned} \kappa_T &= 7 \times 10^{-5} \ln(T) + 7 \times 10^{-5} \text{ MPa}^{-1}, \\ \alpha_p &= 10^{-6} \times T^{1.95} \text{ K}^{-1}. \end{aligned} \quad (8)$$

The pressure is obtained via an integration of Eq. (7), where the integration is done separately for each point in space time, going from room temperature to the temperature of that point. This accounts for the pressure  $P(z, t)$  in the material, and its change over time.

Once the pressure  $P(z, t)$  is obtained, the specific volume can be computed using in addition experimental data displayed in Fig. 2 and fitted in Eq. (2). Integrating along the  $z$ -axis, starting at depth of 21 nm (just beneath the hardened polymer shell) yields the overall final specific volume  $V_s(t)$  of the specimen as a function of time,

$$V_s(t) = \frac{V_{s0} \int_{z_{\text{max}}}^{z_{\text{min}}} \exp\left[-\frac{P(z, t)}{P_0}\right] dz}{z_{\text{max}} - z_{\text{min}}}, \quad (9)$$

with  $z_{\text{min}}=21$  nm, the depth where the unhardened material starts, and  $z_{\text{max}}=250$  nm being the depth of the polymeric layer thickness. The values  $V_{s0}=8.04 \times 10^{-4}$  m<sup>3</sup>/kg and  $P_0=5000$  MPa are the same ones used as fit parameters in Eq. (2).

## III. DISCUSSION

### A. Numerical results

As mentioned above, the thermal diffusivity and thermal conductivity of PMMA have a wide range of values, as experimental results vary according to the specific PMMA melt. The resultant temperature  $T(z, t)$  with the midrange pa-

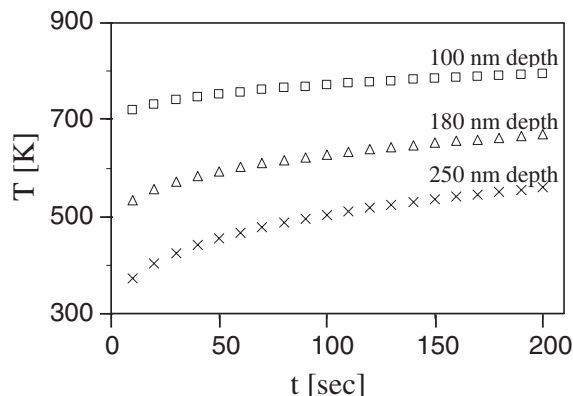


FIG. 6. Heat diffusion gradient in polymeric material as derived by our model with  $\alpha_p=7 \times 10^{-5} \text{ K}^{-1}$ ,  $\kappa_T=2.09 \times 10^{-10} \text{ W nm}^{-1} \text{ K}^{-1}$ . The graph shows the temperature rise as function of time for three different depths into the 250 nm film: 100 nm ( $\square$ ), 180 nm ( $\Delta$ ), and 250 nm ( $\times$ ).

rameters is displayed in Fig. 6. In order to simplify the figure, the temperature is presented as a function of time at three different film depths  $z=100, 180,$  and  $250 \text{ nm}$ .

It should be noted that at small depths even the first temporal results ( $t=10 \text{ s}$ ) have already a very high temperature  $T \approx 700 \text{ K}$  (compared to initial conditions of room temperature). This sudden  $T$  rise at the onset of the process is due to the temporal step function in the model setup, as at  $t=0$  the full power is set (in this setup,  $Q(z)$  is not a function of time).

The next step is to find the pressure profile  $P(z, t)$  from Eq. (7), displayed in Fig. 7 for the same depths as in Fig. 6. The ability of the shell to withstand the elevated pressure was tested using Von-Mises (or maximal allowed deformation energy) criterion of material failure.<sup>37</sup> Calculating the volume loss requires integrating the pressure along the  $z$ -axis according to Eq. (9). It results in dependence of specific volume  $V_s(t)$  on exposure time. The results for this integration are described in Fig. 8 and can be fitted by an exponential decay,

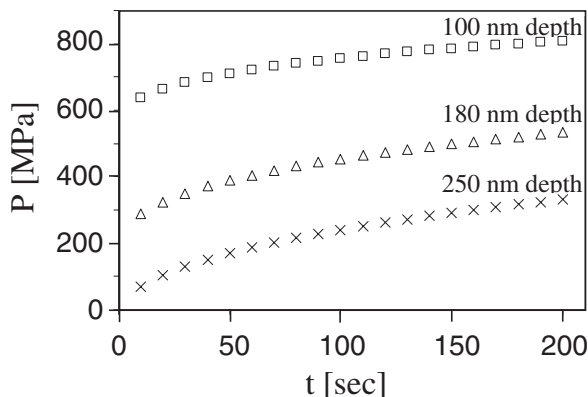


FIG. 7. Pressure gradient in polymeric material as derived by integrating the thermodynamic functions using  $\alpha_p=7 \times 10^{-5} \text{ K}^{-1}$ ,  $\kappa_T=2.09 \times 10^{-10} \text{ W nm}^{-1} \text{ K}^{-1}$ . The graph shows the pressure rise as function of time in three different depths, inside the 250 nm film: 100 nm ( $\square$ ), 180 nm ( $\Delta$ ), and 250 nm ( $\times$ ).

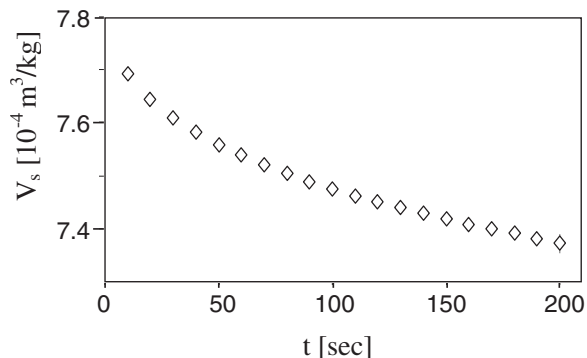


FIG. 8. Calculated dependence of specific volume of PMMA on exposure time to electron radiation.

$$V_s = V_{s0} \left[ 1 + a_2 \exp\left(-\frac{\ln 2}{\tau_2} t\right) \right], \quad (10)$$

with  $a_2 = \frac{1}{16} \approx 0.06$  and  $\tau_2 = 82.5 \text{ s}$ .

## B. Review of experimental results

We shall now return to the experimental data presented in Sec. I. Depending on the specific material, Kudo *et al.*<sup>6</sup> calculated the loss of linewidth through the annealing process to be about 8%–14% of the linewidth. We further assumed (based on partial experimental evidence) that the relative loss in the  $z$ -axis is similar to the width loss along the  $x$ -axis  $W$ . Translating this width loss  $W$  to relative volume loss gives

$$\begin{aligned} \Delta V &= XYZ - X(1-W)Z(1-W)Y, \\ &= V(2W - W^2), \end{aligned} \quad (11)$$

where  $V=XYZ$  is the initial volume and  $\Delta V$  is volume change. As  $W$  is much smaller than unity (its value is about 0.08–0.14), the  $W^2$  term can be neglected,

$$\Delta V \approx 2W \times V \quad (12)$$

and

$$\delta V = \Delta V/V \approx 2W \quad (13)$$

indicates the relative volume loss.

This reduction in width would translate into a 15%–30% ( $\delta V \approx 0.15$ – $0.3$ ) loss in volume. In the same study it was also shown that using a more volatile solvent decreases  $\delta V$  by a factor of 2. In another paper,<sup>4</sup> it was shown that preconditioning of the material decreases  $\delta V$  to about 0.75 of its original value.

To the best of our knowledge, there are no published studies describing systematic attempts to change the solvent as well as precondition the polymeric film before exposure to SEM. Furthermore, there is no evidence that these two effects can be added independently, as both of them tend to affect the phenomenon in the same way by removing solvent remnants. However, as an upper bound for the annealing phenomenon, we will take these effects to be additive, and consider the “pure” effect ascribed to annealing to be 5%–10% of the original width, which constitutes for at least 10% loss of volume.

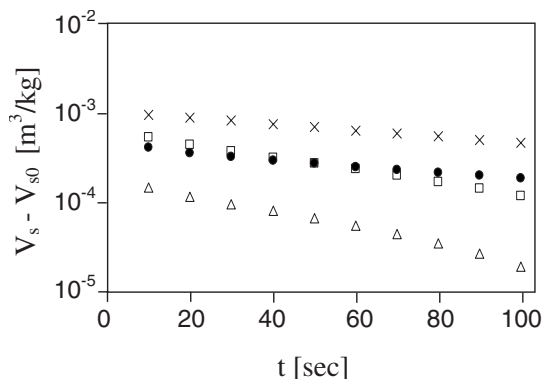


FIG. 9. Model results on semilogarithmic plot, with two variances compared to experimental data. (×) denotes adaption of experimental data (combined from Refs. 4 and 6), (●) marks our model results, (□) indicates a model variance with twice the electron flux, and (△) marks a model variance with half the electron flux.

According to Kudo *et al.*,<sup>6</sup> changing the solvent to a more volatile one will cause less solvent remnants to remain in the resist, resulting in the half-life time of the annealing can be increased from  $\sim 35$  to  $\sim 90$  s: We proceed by comparing to experimental results of both the standard and the more volatile solvents.

### C. Comparison of model and experiment

As described in Secs. I and III B, the line slimming is characterized by three distinct processes [Eq. (1)] and only the second one is related to polymer annealing.<sup>4,6,7</sup> Therefore, taking into account only the polymer annealing would reduce Eq. (1) to

$$V_s/V_{s0} = 1 + a_2 \exp\left[-\frac{\ln 2}{\tau_2} t\right]. \quad (14)$$

$V_{s0}$  is the specific volume in the beginning of the annealing process. Because of the separation of temporal time scales of the three processes in Eq. (1),<sup>6</sup>  $V_{s0}$  can be safely considered as a constant over time scale characterized by  $\tau_2$ . Hence, from the experimental data fit  $a_2$  is measured to be at least  $a_2 > 0.1$  and  $\tau_2$  ranges between  $30 \text{ s} < \tau_2 < 90 \text{ s}$ .

The experiment values have to be compared to the results obtained in the model [Eq. (10)],

$$a_2 = \frac{1}{16}, \quad \tau_2 = 82.5 \text{ s}, \quad (15)$$

and indicate qualitative agreement between the two. As to quantitative agreement, we note that the higher bound of typical times seen in experimental data,  $\tau \approx 90$  s, is somewhat higher than our model results of  $\tau = 82.5$  s. However, there is no quantitative agreement in the value of coefficient  $a_2$  as experimental data give  $a_2 > 0.1$  and our model only reaches  $a_2 \approx 0.06$ . We note that increasing the flux of incoming electrons resulted in even smaller results than those seen in experiments.

The direct comparison of our model and experiments can be seen in Fig. 9. The experimental results show the most pure case of LWS described above. In comparison, the main model results are presented along with two variations in which the incoming electron flux was doubled or halved. The

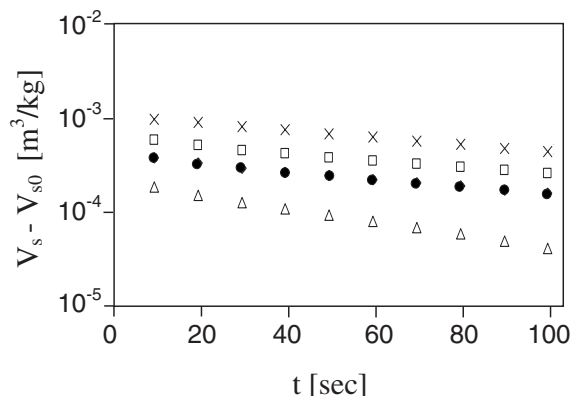


FIG. 10. Model results on a semilogarithmic plot with standard, maximal, and minimal thermal conductivity, compared to experimental data. (×) denotes adaption of experimental data (combined from Refs. 4 and 6), (●) marks our model results with standard  $\kappa_{\text{PMMA}} = 2.09 \times 10^{-10} \text{ W nm}^{-1} \text{ K}^{-1}$ , (□) indicates a model variance with minimal known  $\kappa_{\text{PMMA}} = 1.67 \times 10^{-10} \text{ W nm}^{-1} \text{ K}^{-1}$ , and (△) marks a model variance with maximal known  $\kappa_{\text{PMMA}} = 2.51 \times 10^{-10} \text{ W nm}^{-1} \text{ K}^{-1}$  parameter.

specific volume is plotted on a log scale, after subtracting a constant term representing the two other processes of Eq. (1) not related to annealing.

It is quite clear from Fig. 9 that even when taking electron flux as double their original value (described on the graph as the first variance), there is still no good fit with the experimental results. It should be noted that the electron flux affects both the magnitude of the effect and its temporal coefficient  $a_2, \tau_2$ . From Fig. 10, however, it can be seen that when the model is solved using thermal coefficients on the lower end of their known values, the results approach the experimental ones. Therefore, one of the main conclusions is that the model does not capture in a quantitative way this interesting phenomenon, partially because of the large variation in the thermal coefficients.

A possible cause of this quantitative difference may be related to annealing-stimulated solvent evaporation. This means that solvent molecules that were trapped between polymer chains were “squeezed” out of the polymer through the annealing process—as if they were being “wringed from a fabric.” This metaphor offers a rather good description, as small molecules caught inside a material made of long chains are pushed out. This explains how the solvent still has an effect on the free volume since some molecules are assumed to have been unable to evaporate during baking and other processes intended for solvent removal. Such a plausible explanation requires future studies, and could be a good explanation of the discrepancy because free volume in polymeric material highly depends on the presence of solvent.

As seen in Fig. 10, specific material properties (thermal coefficients, thermal expansion, material free volume, etc.) may have profound impact on the quantitative results of the model. Therefore, the discrepancy between model and experiment may reflect the difference in material properties between the well-studied PMMA and other methacrylates used for photoresists, for which much less data are available.

#### IV. CONCLUSIONS

In this article we approached the issue of photoresist line-width change during SEM inspection, known as LWS or CD Shrinkage, from a purely fundamental point of view. Our goal was to attribute a peculiar effect found in microelectronics manufacturing to the problem of free volume in polymeric materials under pressure.

The free volume of a polymeric material corresponds to the unoccupied regions (voids) accessible to segmental motions and plays an important role in understanding its electrical, mechanical, and transport properties. As mentioned in Sec. II A, free volume has strong effects on mechanical properties of polymer glasses, such as Young's modulus and material hardness. Similarly, it has a strong effect on liquid polymers (melts), affecting their viscosity, glass transition temperature, and other parameters.

In this article we describe an analytical model for the second stage of LWS, in order to check the applicability of polymer annealing to this issue. Using PMMA attributes (for their availability and accuracy) and setup typical of commercial CD-SEMs, we propose a model of polymer shrinkage that loses specific volume with an amplitude of 0.06 (relative units) and a half life of 82.5 s. This is compared to experimental results, in which the amplitude is at least 0.1 and the half life ranges between 30 and 90 s. Therefore, we conclude that our model can explain qualitatively the experimental results, but the quantitative agreement between the model and experiments is only partial. Agreement is reached on the temporal dependency, but with an amplitude that is twice as large in experiment than in the model.

We ascribe two main reasons for this discrepancy. The first is the material differences between PMMA that we used and other methacrylates used for photoresists (and, therefore, in experiments). The second is remnants of solvent caught between the polymer chains in a way that they are trapped and do not evaporate during solvent-removal steps. This way, both the effective free volume and its sensitivity to applied pressure are largely increased.

Possible experimental studies to test this theory would be to take the resist after several rigorous solvent-removal activities, such as long bake in high temperature or exposure to high vacuum, and expose it to SEM radiation. While measuring its shrinkage again, search for evidence of evaporation in the SEM vacuum chamber. Another possibility is to perform direct experimental tests for polymer annealing in "shrunk" photoresist. Such tests could be made using positron annihilation spectroscopy, which are the most widely accepted method of direct free volume measurement. Another option is using AFM density measurements on deep polymer in-material layers in order to probe penetration to material and measuring atomic force inside it.

#### ACKNOWLEDGMENTS

The authors would like to thank M. Murat and A. Drozdov for helpful discussions and suggestions. Support from the Israel Science Foundation (ISF) under Grant No.

231/08 and the U.S.-Israel Binational Foundation (BSF) under Grant No. 2006/055 is gratefully acknowledged.

- <sup>1</sup>R. R. Kunz and R. R. Dammel, SPIE's 28th Annual International Symposium on Microlithography, 2004.
- <sup>2</sup>L. Peters, *Semicond. Int.* **25**, 63 (2002).
- <sup>3</sup>A. Hand, *Semicond. Int.* **23**, 38 (2000).
- <sup>4</sup>L. Pain, N. Monti, N. Martin, V. Tirard, A. Gandolfi, M. Bollin, and M. Vasconi, *Proc. INTERFACE* **2000**, 233 (2000).
- <sup>5</sup>C. H. J. Wu, W. S. Huang, K. J. R. Chen, C. N. Archie, and M. E. Lagus, *Proc. SPIE* **4345**, 190 (2001).
- <sup>6</sup>T. Kudo, J. Bae, R. R. Dammel, W. Kim, D. S. McKenzie, M. D. Rahman, M. Padmanaban, and W. Ng, *Proc. SPIE* **4345**, 179 (2001).
- <sup>7</sup>K. Nozaki and E. Yano, *Fujitsu Sci. Tech. J.* **38**, 3 (2002).
- <sup>8</sup>F. Schrepel, Y. S. Kim, and W. Witthuhn, *Appl. Surf. Sci.* **189**, 102 (2002).
- <sup>9</sup>G. U. Losi and W. G. Knauss, *Polym. Eng. Sci.* **32**, 542 (1992).
- <sup>10</sup>L. C. E. Struik, *Physical Ageing in Amorphous Polymers and Other Materials* (Elsevier, Amsterdam, 1978).
- <sup>11</sup>R. M. Shay and J. M. Caruthers, *Polym. Eng. Sci.* **30**, 1266 (1990).
- <sup>12</sup>J. Mijovic, L. Nicolais, A. D'Amore, and J. M. Kenny, *Polym. Eng. Sci.* **34**, 381 (1994).
- <sup>13</sup>J. J. Curro and R. J. Roe, *Polymer* **25**, 1424 (1984).
- <sup>14</sup>J. M. Hutchinson and C. B. Bucknall, *Polym. Eng. Sci.* **20**, 173 (1980).
- <sup>15</sup>K. Takahara, H. Saito, and T. Inoue, *Polymer* **40**, 3729 (1999).
- <sup>16</sup>H. Eyring and J. Hirschfelder, *J. Phys. Chem.* **41**, 249 (1937).
- <sup>17</sup>M. H. Cohen and D. Turnbull, *J. Chem. Phys.* **31**, 1164 (1959).
- <sup>18</sup>K. C. Rusch, *J. Macromol. Sci., Part B: Physics* **2**, 179 (1968).
- <sup>19</sup>H. Higuchi, Z. Yu, A. M. Jamieson, R. Simha, and J. D. McGervey, *J. Polym. Sci., Part B: Polym. Phys.* **33**, 2295 (1995).
- <sup>20</sup>R. A. Pethrick and W. J. Davis, *Polym. Int.* **47**, 65 (1998).
- <sup>21</sup>Q. Guo, C. B. Park, X. Xu, and J. Wang, *J. Cell. Plast.* **43**, 69 (2007).
- <sup>22</sup>M. Schmidt and F. H. J. Maurer, *J. Polym. Sci., Part B: Polym. Phys.* **36**, 1061 (1998).
- <sup>23</sup>F. E. Du-Prez, P. Tan, and E. J. Goethals, *Polym. Adv. Technol.* **7**, 257 (1995).
- <sup>24</sup>J. Yang, S. Liu, X. Guo, Y. Luan, W. Su, and J. Liu, *Macromol. Chem. Phys.* **203**, 1081 (2002).
- <sup>25</sup>J. H. R. Clarke, in *Monte Carlo and Molecular Dynamics Simulations in Polymer Science*, edited by K. Binder (Oxford University Press, New York, 1995).
- <sup>26</sup>B. Prathab, V. Subramanian, and T. M. Aminabhavi, *Polymer* **48**, 409 (2007).
- <sup>27</sup>J. M. Caruthers, D. B. Adolff, R. S. Chambers, and P. Shrikhande, *Polymer* **45**, 4577 (2004).
- <sup>28</sup>C. Graf, A. Vath, and N. Nicoloso, *J. Power Sources* **155**, 52 (2006).
- <sup>29</sup>T. Sarubi, M. F. Ross, M. Neisser, T. Kocab, B. T. Beauchemin, Jr., W. R. Livasay, S. S. Wong, and W. Ng, *Proc. SPIE* **4345**, 211 (2001).
- <sup>30</sup>Hitachi High-Technology, CD-SEM Applications Training, version 18, 2007.
- <sup>31</sup>A. G. Deleporte, J. A. Allgair, C. N. Archie, G. W. Banke, Jr., M. T. Postek, Jr., J. E. Schlesinger, A. E. Vladar, and A. W. Yanof, *Proc. SPIE* **3998**, 12 (2000).
- <sup>32</sup>R. D. Larrabee and M. T. Postek, in *Handbook of Critical Dimension Metrology and Process Control*, edited by Kevin M. Monahan (SPIE Critical Review, 1994), Vol. CR52.
- <sup>33</sup>B. Su and O. Harel, *Proc. SPIE* **3998**, 38 (2000).
- <sup>34</sup>L. Akerman, G. Eytan, R. Uchida, S. Fujimura, and T. Mimura, *J. Microolithogr., Microfabr., Microsyst.* **5**, 043005 (2006).
- <sup>35</sup>M. Sambasivam, A. Klein, and L. H. Sperling, *J. Appl. Polym. Sci.* **65**, 1001 (1997).
- <sup>36</sup>C. Kittel and H. Kroemer, *Thermal Physics*, 2nd ed. (Freeman, San Francisco, 1980).
- <sup>37</sup>Materials Datasheets, www.efunda.com, Engineering Fundamentals.
- <sup>38</sup>S. Goswami and D. Chakrabarty, *J. Appl. Polym. Sci.* **93**, 2764 (2004).
- <sup>39</sup>J. H. Mathews and D. F. Kurtis, *Numerical Methods Using MATLAB*, 3rd ed. (Prentice-Hall, Upper Saddle River, NJ, 1999).
- <sup>40</sup>S. B. Sane, T. Cagin, W. G. Knauss, and W. A. Goddard, *J. Comput.-Aided Mater.* **8**, 87 (2001).